Microchimica Acta (2020) 187: 635
https://doi.org/10.1007/s00604-020-04614-y

ORIGINAL PAPER

Impedimetric DNA E-biosensor for multiplexed sensing of *Escherichia coli* and its virulent *f17* strains

Amal Rabti[1] · Riham Zayani[1] · Marwa Meftah[1] · Imed Salhi[2] · Noureddine Raouafi[1]

Received: 1 July 2020 / Accepted: 21 October 2020 / Published online: 3 November 2020

Abstract

An impedance-based DNA multiplexed biosensor was designed to simultaneously detect *Escherichia coli* (*yaiO* gene) and its virulent *f17* variant. The thiolated DNA dual probe was self-assembled onto the surface of the gold nanoparticle-modified screen-printed carbon electrode (AuNPs/SPCE) to recognize selected sequences from *yaiO* and *f17* genes. The optimal conditions to prepare the bioelectrode were determined based on the monitoring of the impedimetric response fitted to an equivalent electrical circuit model. The charge transfer resistance of the bioelectrode increased by recognizing the target DNA sequences. The limit of detection was 0.8 fM and 1.0 fM for *yaiO* and *f17* target DNA, respectively, and the linearity ranged from 1×10^{-15} to 1×10^{-7} M with a linear regression coefficient $R \geq 0.995$. The nanodevice provided a novel strategy for simultaneous detection of *E. coli* and its virulence *f17* gene with excellent discrimination with a single-base mismatch, two-base mismatch, and non-complementary sequences. Moreover, genomic DNA extracted from *E. coli* bacteria isolated from diarrheic camel calves and control animals in Tunisia was successfully detected using the as-prepared biosensor with minimal treatment of the extracted DNA samples.

Keywords Dual biosensor · Impedance spectroscopy · Pathogen · *Escherichia coli* · F17 fimbriae · Multiplexing

Introduction

Toxins, adhesins, and invasion factors are virulence factors produced by pathogenic variants ofbacteria. Fimbrial and afimbrial adhesins enable enterotoxigenic *Escherichia coli* (ETEC) to colonize the gastrointestinal tract of the hosts and are involved in the onset of extra-intestinal infections caused by ETEC released toxins [1]. Among them, the *f*17-related fimbriae family mediates binding to receptors containing *N*-acetyl-D-glucosamine, which are located at intestinal mucosal cells and bovine erythrocytes. It also mediates in vitro adhesion to bovine intestinal brush borders or to the human Caco-2 cell line [2]. Furthermore, *f*17 fimbriae are frequently diagnosed in ETEC strains isolated from diarrheagenic and septicemic various animal species. For example, it is involved in diarrhea among camel in Tunisia [3] and in calves' illness throughout Uruguay [4]. Moreover, the F17 fimbriae family is also related to the incidence of bovine mastitis, which is a serious problem for the worldwide dairy industry [5].

Because of their important role as targets for therapeutic intervention such as vaccines, differentiation of various fimbriae of ETEC and their simultaneous analysis remain a challenging task. PCR-based assays were used for the identification of *f*17 [6] and other virulence fimbrial subtypes genes [7, 8]. Moreover, the multiplex PCR method based only on two runs of amplification allowed the detection of all the F17-related fimbriae, i.e., F17a, F17b, F17c, F111, and G fimbriae, and the identification of four subtypes of structural sub-unit genes and two distinct subfamilies of adhesin genes [2]. Another approach, consisting of developing an *E. coli* virulence factor DNA microarray was investigated to detect the pathogenic potential of *E. coli* [9]. Loop-mediated isothermal amplification procedure was also explored for the determination of the *f5* gene in ETEC with a detection limit of 72 cfu/tube, which was greater than that obtained with PCR (7.2×10^2 cfu/tube) [10]. Nevertheless, these techniques are time-wasting and need special instruments and skilled personals, thus restricting their extensive practical application.

Supplementary Information The online version contains supplementary material available at https://doi.org/10.1007/s00604-020-04614-y.

✉ Noureddine Raouafi
noureddine.raouafi@fst.utm.tn

[1] Sensors and Biosensors Group, Analytical Chemistry and Electrochemistry Lab (LR99ES15), Faculty of Science, University of Tunis El Manar, 2092 Tunis El Manar, Tunisia

[2] Livestock and Wildlife Laboratory (LR16IRA04), Arid Lands Institute (I.R.A), University of Gabès, Medenine, Tunisia

Electrochemical genosensors, allowing simultaneous analysis of several biomolecules, have attracted much interest to develop multiplexed point-of-care testing (POCT) devices because of their cost-effectiveness, amenability, and little bit sensitivity towards the matrix effects compared to other analytical methods. Among them, multiplexed biosensors using dual SPCE were developed to simultaneously detect tumor biomarkers [11]. Taken advantage of nanoparticles and nanostructures [12, 13], multiplexed electrochemical assays were also achieved with a modified single working electrode. In fact, using labeled probes with multi-signal output [14] or functionalized metal-organic frameworks with dsDNA and electroactive dyes, i.e., MB and TMB, which are susceptible to be released and detected after hybridization with target miRNAs [15], were some of the used approaches to design sensitive multiplexed biosensors. For instance, Chen et al. [16] reported a bovine serum albumin-dual-probe genosensor using only one probe, instead of double probes, to discriminate dominant hepatitis B virus genotypes B and C by measuring two readings at two different temperatures. Xu et al. [17] designed a DNA circle capture probe attached to a DNA nanometric structure to detect miRNA-21 and miRNA-155 simultaneously using helper strands. However, these assays suffer from one of the following drawbacks such as the usage of various capture probes, engendering crowding or steric effect and nonspecific interactions between probes, the need for secondary labeling with nanoparticles or label carriers, and the dependence of some of these biosensors on signal amplification strategies using enzymes, which increased the assay duration and cost. Moreover, although a multiplexed electrochemical survey was carried out for simultaneous recognition of *E. coli* O157:H7 and either *Staphylococcus aureus* [18] or *Vibrio cholerae* O1 [19], no DNA-based electrochemical biosensors were reported for the simple or simultaneous detection of different fimbriae produced by pathogenic *Escherichia coli*.

Considering all the mentioned above and taking advantage of EIS as a sensitive label-free assay, a new impedimetric DNA dual biosensor was developed for the simultaneous determination of *E. coli* (*yaiO* gene) and its virulent *f17* fimbriae. After nanostructuration of SPCE with gold nanoparticles (AuNPs/SPCEs), the thiolated DNA dual-probe sequence was self-assembled using a potential pulse-assisted procedure. The hybridization of the probe with complementary targets from *yaiO* and *f17* genes was detected by EIS. The changes of the electrode interfacial surface properties following DNA immobilization and hybridization were monitored by registering the charge transfer resistance (R_{ct}), which was adopted as the signal for label-free detection of targets DNA. The bioelectrode allowed discrimination between *E. coli* strains positive and negative for *f17* fimbriae. Moreover, its practical application was confirmed by the successful detection of genomic DNA from *E. coli* strains isolated from diarrheic and healthy camel calves in Tunisia. Given what we know, there is no previous research dealing with the use of neither the *yaiO* gene for electrochemical detection of *E. coli* nor electrochemical DNA biosensor for virulent *f17* fimbriae detection. Furthermore, this designed label-free electrochemical dual biosensor presents a perfect platform for POC applications when combined with portable instrumentation. No treatment was needed for detection of genomic DNA of the *E. coli*.

Experimental

Apparatus and electrodes

A Metrohm PGSTAT M204 potentiostat fitted with a FRA32 impedance, controlled by Nova® software (v2.1.3), was used to record all the electrochemical measurements. Screen-printed carbon electrodes (SPCEs OHT-000), where carbon material is used to make the working (4-mm diameter) and counter-electrodes and the pseudo-reference electrode is a silver-based electrode, were purchased from Orion Hi-Tech S.L. (www.orion-hitech.com) (Madrid, Spain). Moreover, free web-based analysis tool OligoAnalyzer software 3.1 (https://eu.idtdna.com/) was used to estimate the free energy (ΔG) related to the formation of the hairpin structure by the DNA probe and the free energy associated with each target hybridization step.

Chemicals and solutions

The reagents used were of the highest analytical grade: 6-mercaptohexanol (MCH, 99%), tris-(hydroxymethyl)aminomethane chloride (Tris-HCl, 99%), ethylenediaminetetraacetic acid (EDTA, 99%), tris(2-carboxyethyl)phosphine hydrochloride (TCEP, 98%), tetrachloroauric acid trihydrate ($HAuCl_4 \cdot 3H_2O$, 99.9%), H_2SO_4 (95%), HCl (37%), NaCl (99%), K_2SO_4 (99%), $K_4Fe(CN)_6 \cdot 3H_2O$ (99%), and $K_3Fe(CN)_6$ (99%) were purchased from Sigma-Aldrich (www.sigmaaldrich.com) (Germany).

Milli-Q water (18 MΩ cm at 25 °C) was used to prepare all the buffer solutions. Buffer solutions used include buffer 1 composed of 10 mM Tris-HCl supplemented with 1 mM EDTA and 0.3 M NaCl (Tris-EDTA buffer) of pH 8.0; buffer 2 formed of 0.01 M phosphate buffer solution containing 150 mM NaCl and 450 mM K_2SO_4 of pH 7.4. Other solutions/suspensions employed include a 0.01 M phosphate buffer solution (pH 7.4) containing 20 mM K_2SO_4 and 5 mM $K_3Fe(CN)_6/K_4Fe(CN)_6$ (1:1) (measurement solution); a 1 mM $HAuCl_4$ solution prepared in 0.1 M HCl.

Table S1 (supplementary material) summarizes the sequences of all the used synthetic oligonucleotides DNA. All these polynucleotide acid, received from Biomers.net GmbH (www.biomers.net) (Germany), were dissolved in RNase-free water to obtain a 100 μM final concentration. Aliquots were prepared and maintained at − 80 °C.

Methods

Electrodeposition of gold nanoparticles

Prior to use, SPCEs were pre-treated according to the previous report [20] in order to increase the surface functionalities by removing the organic ink constituents or contaminants. Three pre-treatment procedures were considered (Fig. S1 in the Supplementary material), and one of them was chosen. Briefly, 10 scans of CV were registered in a potential window from − 0.5 to + 1.0 V with a scan rate of 50 mV s^{-1} after placing 50 μL of PBS over the SPCE. Following this pre-treatment, gold nanoparticles were deposited over SPCEs (AuNPs/SPCEs) according to modified literature [21]. In 1 mM $HAuCl_4$ acidic solution, the application of a constant current intensity of − 100 μA for 240 s and subsequently by applying a potential of + 0.1 V for 120 s was carried out. The nanostructured SPCEs were generously washed with ultrapure water and left to dry at room temperature (RT). An activation step in sulfuric acid was primordial before use to remove the AuNPs oxidation layer and thus exposing more active sites on the electrode surfaces, which will enhance its electrochemical performances [12]. To do so, AuNPs/SPCEs underwent 20 subsequent CV runs from 0.0 to + 1.2 V at a scan rate of 100 mV s^{-1} in 0.5 M H_2SO_4 [22]. The fabricated AuNPs/SPCEs were electrochemically characterized by CV in 0.5 M H_2SO_4 and in the measurement solution (Fig. S2).

Immobilization of the thiolated DNA probe

Firstly, 100 μL of 10 μM capture probe DNA was treated with 0.5 μL of 2 M TCEP for 1 h to cleave the disulfide bonds. Then, a potential pulse-assisted process based on switching the applied potential between + 0.5 V and − 0.2 V with a 10-ms pulse duration in a DNA probe solution (prepared in buffer 2) was applied to immobilize the DNA probe onto AuNPs/SPCEs surfaces [23]. Both the impact of the duration of these pulses and the DNA probe concentration were studied as well.

After thoroughly washing with water, the probe-modified electrodes were eventually incubated in 0.1 mM MCH aqueous solution (prepared in buffer 2) for 5 min to reduce non-specific adsorption [24]. For comparison, passive chemisorption of the capture probe was studied by casting 10 μL of 0.5 μM probe solution (prepared in buffer 2) over the working electrode and incubating overnight at 4 °C in a humidified chamber.

Hybridization of target DNA

Recognition of target DNA sequences was achieved by dropping various concentrations of *f17*, *yaiO*, or *yaiO/f17* mixture DNA solutions (prepared in buffer 2) onto the modified SPCEs and incubation for 5 min at RT. Then, the non-hybridized sequences were removed by washing with ultrapure water. To study the biosensors selectivity, the same procedure was conducted with *f17* single-base mismatch, *yaiO* two-base mismatch, and non-complementary targets DNA.

Isolation of *E. coli* strains, fragmentation, and PCR assays

A strain isolated from diarrheic camel calf with the virotype *f17/afa/EastI/papC/iroN/iss/iucD* and serotype O64 and belonging to the phylogenetic group B1 served as a positive control for the *f17* gene and the TG1 strain was employed as a negative control [3]. DNA was extracted by boiling. In fact, bacteria were pelleted from 1.5-mL LB broth overnight culture at 37 °C, suspended in 200 μL sterile distilled water, and boiled at 100 °C for 10 min. The supernatant obtained after centrifugation of the lysate at 12,000*g* for 15 min was employed as a PCR template.

For the fragmented DNA assay, the whole DNA was digested by 20 units of NotI restriction enzyme for 4 h at 37 °C. The *f17* virulence gene was detected using a uniplex PCR assay according to the OIE Reference Laboratory protocol for *Escherichia coli* (EcL-Faculté de Médecine Vétérinaire, Université de Montréal) [3].

Detection of genomic DNA

Hybridization with genomic DNA before and after digestion with restriction enzyme was performed by dropping 10 μL of DNA solutions onto the modified SPCEs and incubation for 5 min at RT. Then, the non-hybridized sequences were removed by washing with ultrapure water.

Electrochemical impedance spectroscopy measurements

Fifty microliters of the measurement solution was placed onto the surface of the electrode after each modification step of the SPCE, and the frequency was varied from 100 kHz to 0.10 Hz at an applied potential of 0.0 V vs. Ag/AgCl, with amplitude modulation of 0.2 V. Nyquist plots were fitted to the modified Randles equivalent circuit [$R_s(Q[R_{ct}W])$] where R_s is the solution resistance; Q is the constant phase element; R_{ct} is the charge transfer resistance; and W is the Warburg impedance. To minimize the variability, the variation of the charge transfer resistance (ΔR_{ct}) obtained after performing electrochemical assays with a fixed concentration of DNA targets was evaluated as the analytical response. ΔR_{ct} is calculated from the equation $\Delta R_{ct} = R_{ct}(\text{before}) - R_{ct}(\text{after})$, where R_{ct}(before) and R_{ct}(after) refer to the R_{ct} values obtained before and after each modification step, respectively.

Results and discussion

Design of the biosensor

Simultaneous detection of *Escherichia coli* DNA and its virulent *f17* strain was achieved using a DNA dual biosensor described in Scheme 1. A nanostructured screen-printed electrode was modified by tethering a thiolated DNA capture probe (HS-DNA) composed of two sequences. In fact, the 51 base pairs HS-DNA probe was designed to be complementary to two 20 nucleotides sequence from the orphan gene *yaiO* and the virulence *f17* gene, respectively. The orphan gene *yaiO*, expressed and localized in the outer membrane protein-encoding sequence of the *E. coli* genome, was chosen because it is preserved throughout various lineages of *E. coli* and is not common in other foodborne pathogens according to BLAST analysis [25]. Moreover, it was proven that its amplification is specific for *E. coli* [26]. The major sub-unit of the F17a pili sequence was selected as target DNA for F17-related fimbriae. Subsequently, MCH was self-assembled onto the modified electrode to minimize nonspecific adsorption, allowing the assembled probes to "stand up" and thus achieving better hybridization with the DNA targets [24]. The HS-DNA/target DNA duplex was formed after the addition of DNA target sequences, i.e., *yaiO* or *f17* or their mixture. The changes of the SPCE surface after each modification steps were investigated using EIS, which was adopted as the analytical signal.

It is worth mentioning that the hairpin formation by the long DNA probe may hamper the hybridization with the targets and thus requires thermal pre-treatment to denature and fully break its secondary conformation. From a thermodynamic point of view, temperature-dependent Gibbs energy could give the most stable hairpin structure at a given temperature, and hence, the temperature needed to overcome potential hairpin formation and self-dimerization could be simply predicted [27]. The calculated ΔG value for hairpin structure formation by the DNA probe was -1.95 kcal mol^{-1} at RT, which indicated the absence of hairpin formation and so the developed assay was carried out without heat pre-treatment. Furthermore, ΔG values related to the hybridization of target DNA sequences, i.e., *yaiO* or *f17* or an equimolar mixture of both, were respectively -40.61, -39.38, and -41.95 kcal mol^{-1}. These results clearly confirmed the strong coupling of the designed HS-DNA probe with target DNA sequences.

The realization of the dual biosensor was evaluated by EIS characterization. As can be seen from Fig. 1, the enlarged semicircle of SPCE (curve a) with a R_{ct} equal to $406.7 \pm 4.4\ \Omega$ ($n = 3$) disappeared to give a very small semicircle (curve b) while the R_{ct} value decreased significantly to $\sim 148.7 \pm 5.1\ \Omega$ after modification with AuNPs. The presence of AuNPs induces improvement of both conductivity and electron transfer (ET) process, which was consistent with CV measurements (Fig. S2B). In fact, the enhancement of the electroactive surface area, estimated using Randles-Sevcik formulae [28], from 0.112 cm^2 for unmodified SPCE to 0.133 cm^2 for AuNPs/SPCE was in good agreement with the observed better electrical conductivity. When the HS-DNA probe was tethered on the electrode (curve c), the R_{ct} increased to $405.4 \pm 3.4\ \Omega$ thanks to the repulsive reaction between negatively charged HS-DNA/AuNPs/SPCE surfaces and the redox ferricyanide/ferrocyanide ions. Subsequently, the electrode was backfilled with MCH (curve d) and a larger R_{ct} ($R_{ct} = 564.7 \pm 2.6\ \Omega$) was generated due to the MCH insulating properties and to their ET blocking effect. Next, the R_{ct} value further increased ($R_{ct} = 959.0 \pm 3.7\ \Omega$) after incubation of *yaiO* target DNA (curve e) as the generation of the *yaiO*/HS-DNA duplex decreased the electron transfer efficiency of the redox mediator. These results proved the successful assembly of the dual biosensor.

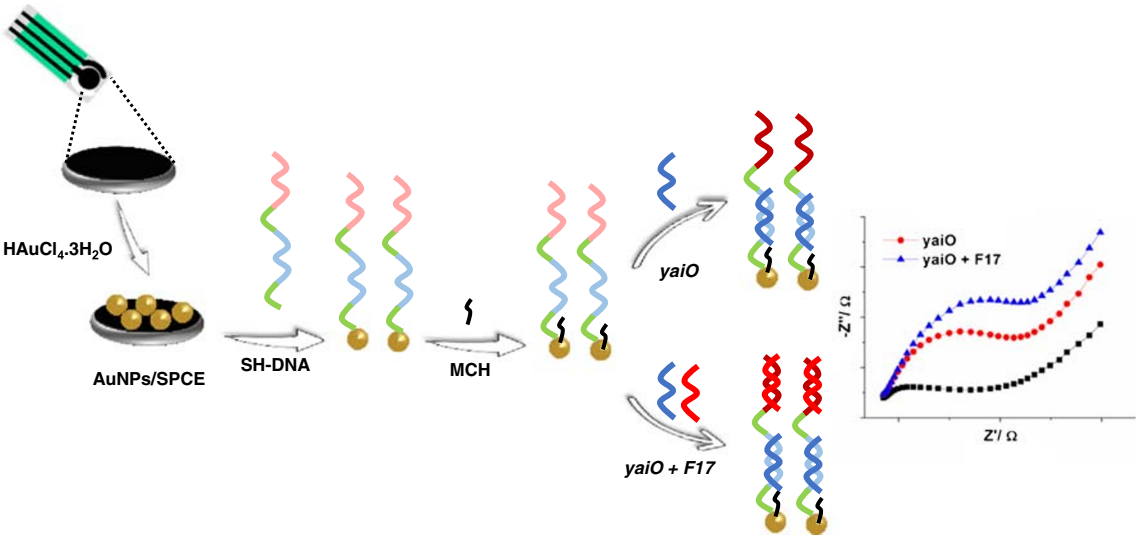

Scheme 1 Fabrication process of the DNA dual biosensor for simultaneous determination of *Escherichia coli* DNA and its virulent *f17* strain

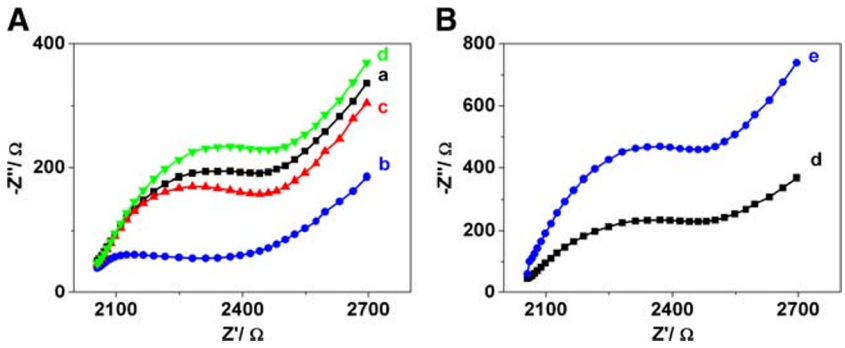

Fig. 1 (**z**) Nyquist plots recorded in buffer 2 of (a) bare SPCE; (b) AuNPs/SPCE; (c) HS-DNA/AuNPs/SPCE; (**b**) MCH/HS-DNA/AuNPs/SPCE before (d) and after (e) hybridization of 100 pM *yaiO* target DNA

Optimization steps of the dual biosensor

To experimentally establish the fittest parameter to achieve the dual biosensor, high performances, the capture probe assembly time and concentration, and the time needed for target DNA hybridization were optimized. All these variables were optimized by comparing the difference between the R_{ct} measured before and after assembly of the capture probe DNA or hybridization with 100 pM of *f17* target DNA.

Immobilization of the capture probe

Potential pulse-assisted technique consisting of repetitive switching between positive and negative potentials with a millisecond rate (+ 0.5 V/− 0.2 V, potential pulse duration 10 ms) allowed the fast and controllable preparation of self-assembled monolayer of thiolated DNA onto gold electrode [29, 30]. To immobilize the capture probe DNA, the effect of the procedure duration on the HS-DNA loading was studied. In fact, different durations ranging from 30 to 600 s were tested and the corresponding ΔR_{ct} values were recorded. As it can be seen from Fig. S3A, ΔR_{ct} obtained after binding of HS-DNA (0.5 μM), gradually increased with increasing the time scale of the process up to 300 s and then plateaued, which indicates that the saturation point was reached. A 300-s total duration of these pulses was then selected as optimum since it yielded the highest HS-DNA coverage.

To further investigate the potential-assisted immobilization, a comparison with passive chemisorption, where the electrode was incubated in a HS-DNA solution overnight, was examined. Figure S3B showed that the immobilization time greatly increased by a factor of 288 in comparison to the potential pulse-assisted method and demonstrated a ~ 0.3-fold ΔR_{ct} decrease for passive adsorption. In fact, using the incubation method is known to exhibit slow kinetics, demanding hours to days to accomplish the best possible reproducible coverage as a result of the higher electrostatic repulsion between the negatively charged DNA strands [23]. Therefore, the potential pulse-assisted HS-DNA chemisorption, ensuring fully covered surfaces within minutes, was selected for this work.

To identify the optimal concentration of the capture probe DNA, three different concentrations were tested, namely 0.10, 0.25, and 0.50 μM (Fig. S3C). By increasing the HS-DNA concentration, the R_{ct} value of HS-DNA-AuNPs/SPCE increased and ΔR_{ct} value increased, accordingly. This was due to the higher surface coverage of the DNA probe onto AuNPs/SPCE, which hindered the accessibility of the redox probe to reach the working electrode surface. For further studies, 0.5 μM of capture probe DNA concentration was chosen.

Hybridization step

The dependence of the impedance response with the target DNA hybridization time was studied. The *f17* gene (100 pM) served as a model target to measure the total impedance before and after hybridization (Fig. S3D). Obviously, the obtained ΔR_{ct} changed slightly with increasing the hybridization time from 5 to 15 min, indicating that a short time was sufficient for total target hybridization. This was advantageous as others' DNA impedimetric assay required more than 60-min incubation [31]. Thus, the hybridization time for the next experiments was set as 5 min.

Analytical performance

Under the optimal setting, individual detection of *yaiO* or *f17* target DNA was evaluated. The semicircle domain of the Nyquist plot increased proportionally with the increase in *yaiO* or *f17* target DNA concentration (data not shown). In fact, R_{ct} increased from 414.3 to 1034.2 Ω and from 445.7 to 1102.0 Ω with increased *yaiO* or *f17* DNA concentration from 1×10^{-15} to 1×10^{-7} M, respectively (Fig. 2A, B). The changes in the ΔR_{ct} value of different concentrations of the target DNA were illustrated in Fig. 2C, D. A straight with a large dynamic window ranging from 1×10^{-15} to 1×10^{-7} M with a correlation coefficient $R \geq 0.995$ (insets of Fig. 2C, D) was obtained after plotting ΔR_{ct} versus logarithmic target DNA concentration. It is important to mention that the regression equations for individual detection of *yaiO* and *f17* target DNA were comparable, which was expected since the capture probe is formed of (1:1) complementary sequences. The equation

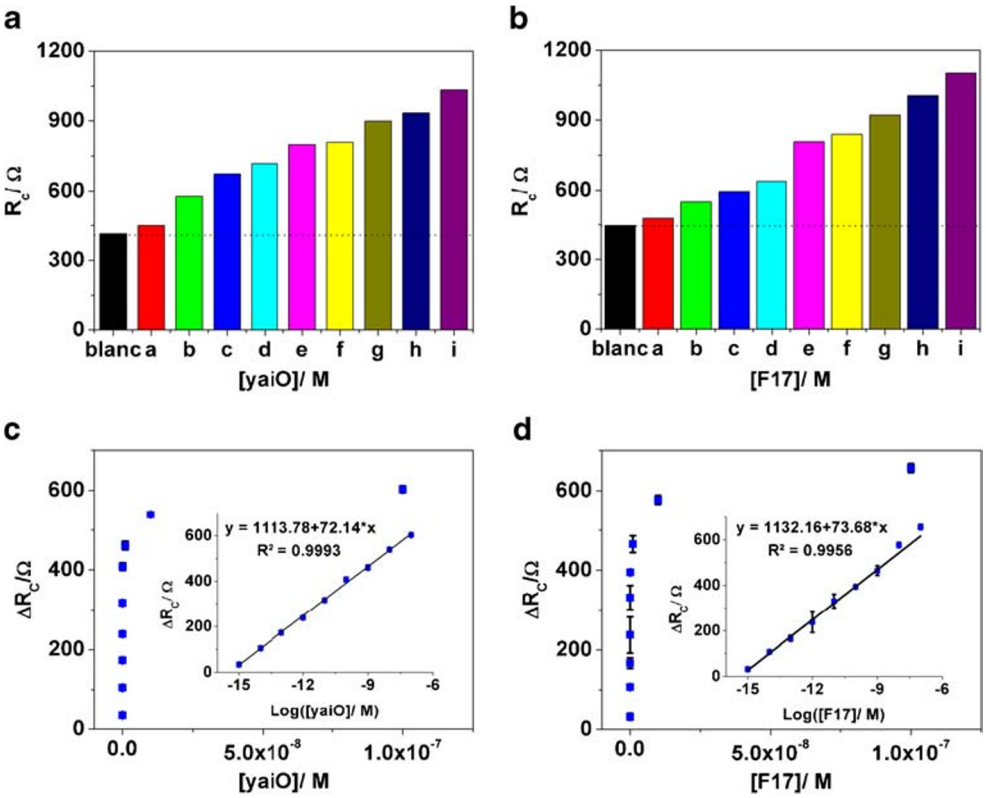

Fig. 2 The value of R_{ct} obtained after detection of various *yaiO* (**a**) and *f17* (**b**) concentrations: (a) 10^{-15} M; (b) 10^{-14} M; (c) 10^{-13} M; (d) 10^{-12} M; (e) 10^{-11} M; (f) 10^{-10} M; (g) 10^{-9} M; (h) 10^{-8} M; and (i) 10^{-7} M; **c** and **d** are related to the calibration curves of ΔR_{ct} vs. [*yaiO*] and [*f17*], respectively; Inset: representations of ΔR_{ct} vs. log [*yaiO*] and log [*f17*], respectively. Error bars, SD, $n = 3$

LOD = 3 × s/m and LOQ = 10 × s/m, where LOD and LOQ are respectively the limits of detection and quantification; *s* is the blank's standard deviation measurements (in the absence of the two targets; $n = 3$); and *m* represents the slope of the calibration equation, were used to estimate these limits. The limits of detection were 0.8 fM and 1.0 fM for *yaiO* and *f17* target DNA, respectively. Moreover, the limits of quantification were estimated to be 5.3 fM and 7.7 fM for *yaiO* and *f17* target DNA, respectively. The obtained wide linear range and low detection limits suggested that the proposed dual biosensor is a promising analytical platform for individual detection of *yaiO* and *f17* target DNAs.

Simultaneous detection of *f17* and *yaiO* target DNAs was further investigated by recording EIS responses of HS-DNA/AuNPs/SPCEs before and after hybridization of different concentration of mixture containing both targeted DNA sequences. Figure 3A and B illustrated that the increase of R_{ct} value was directly related to increased concentrations of complementary targets. A linear dependency of ΔR_{ct} with the log of target DNA concentration ranging from 1×10^{-15} to 1×10^{-7} M (insets of Fig. 3B) was proved, according to the following equation: $\Delta R_{ct}(\Omega) = 2256.3 + 141.9 \times \log C(\text{mol L}^{-1})$, with $R = 0.992$. The calculated LOD and LOQ were equal to 1.0 fM and 133.7 fM, respectively. Consequently, the proposed dual biosensor is capable to differentiate between *f17*-fimbriated *E. coli*, i.e., *E. coli* strains positive for *f17* fimbriae, by detecting the presence of both *f17* and *yaiO* gene oligonucleotides, and *E. coli* not producing the *f17* virulence gene, i.e., *E. coli* strains negative for *f17* fimbriae, by spotting only *yaiO* DNA. However, the determination of the exact concentration of each targeted genes (*yaiO* and *f17*) in real samples is a major limitation of this dual biosensor due to the assumption of an equal amount of both genes in the prepared analyzed samples, which could not be the case in real sample.

Although *yaiO* DNA was only determined using colorimetric [25] and PCR techniques [26, 32] and no DNA-based electrochemical biosensors were recorded for the detection of *yaiO* or *f17* genes, pathogenic *E. coli* detection based on other DNA target sequences were described (Table S2). Our biosensor showed satisfactory analytical performances compared with previous studies. Furthermore, it presented additional advantages namely, the simultaneous detection of tow analytes and the lower assay time for the fixation of the capture probe DNA and for the hybridization process. For example, it achieved better analytical performances when compared with biosensor based only on screen-printed graphite electrode [33] due to the conducting capability and high surface-to-volume ratio of AuNPs plus their favorable biocompatibility and especially their suitability for binding to biomolecules via thiol-gold association. Moreover, although impedimetric biosensor APTMS-ZnO/c-GNF/ITO [34] had lower LOD and wider linear range, our biosensor had a simpler platform without the need to use different nanomaterials and lower assay time, i.e., 5 min instead of 4 h for probe immobilization and 5 min instead of 30 min for the hybridization step. Thus, it can be affirmed that the dual biosensor is desirable for the detection of *yaiO* and *f17* target DNAs with a satisfactory analysis time and good LOD.

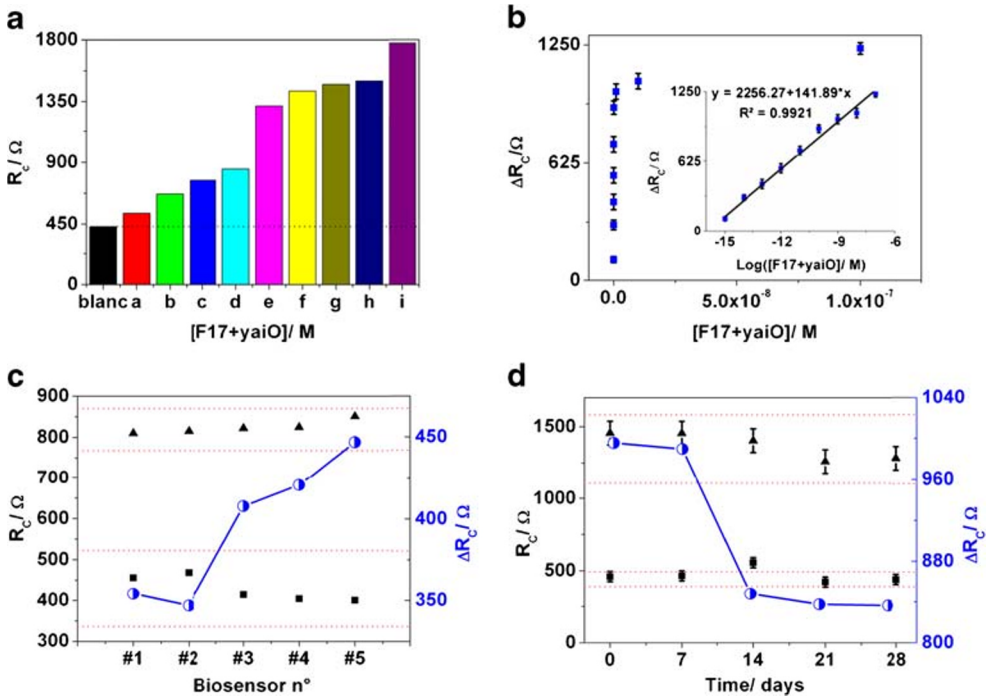

Fig. 3 (**a**) The value of R_{ct} after simultaneous detection of various concentrations of *yaiO* and *f17* strains [*f17*+*yaiO*]: (a) 10^{-15} M; (b) 10^{-14} M; (c) 10^{-13} M; (d) 10^{-12} M; (e) 10^{-11} M; (f) 10^{-10} M; (g) 10^{-9} M; (h) 10^{-8} M; and (i) 10^{-7} M. (**b**) Calibration plot of ΔR_{ct} vs. [*f17*+*yaiO*]; inset: plots of ΔR_{ct} vs. log [*f17*+*yaiO*]. (**c**) The value of R_{ct} before (black square) and after (black triangle) detection of 100 pM *yaiO* strains provided by five independently fabricated biosensors; ± 3 × SD of the mean current values were used as the control limits. (**d**) The value of R_{ct} before (black square) and after (black triangle) simultaneous detection of 100 pM mixture of *yaiO* and *f17* strains provided by stored biosensors at different times; ± 3 × SD of the mean current values registered with four independent biosensors designed on the beginning of the study were used as the control limits. Error bars, SD, $n = 3$

Stability and reproducibility

To study the reproducibility of the dual biosensor, the R_{ct} value of five independently fabricated electrodes was checked before and after hybridization of 100 pM *yaiO* (Fig. 3C). The relative standard deviation was only 3.8%, revealing the biosensors good reproducibility. Moreover, the stability of the proposed biosensor was also examined. Five HS-DNA-AuNPs/SPCEs were designed on the same day, preserved at 4 °C in a dry environment over 1 month and evaluated each week by registering EIS response before and after hybridization of 100 pM mixture of *f17* and *yaiO* target DNAs. As displayed in Fig. 3D, about 91% of the biosensors initial response was retained after 4 weeks, denoting an acceptable shelf-life time.

Selectivity

For evaluation of the biosensor selectivity, the impedance responses registered after the detection of 100 pM of *yaiO* or *f17* or *yaiO/f17* mixture DNA targets were compared to the responses generated after hybridization of the same concentration of single-base mismatch (*f17-1M*), two-base mismatch (*yaiO-2M*), non-complementary DNA, and mixtures of *yaiO/f17-1M*, *f17/yaiO-2M*, and *yaiO-2M/f17-1M* DNA targets. The developed biosensor was able to discriminate complementary targets and mismatched strands (Fig. 4A). Assuming 100% complementary hybridization efficiency for the mixture of *yaiO/f17* genes ($\Delta R_{ct} = 917.9 \pm 35.2$ Ω), almost 50% of the response was obtained after reaction with only *yaiO* ($\Delta R_{ct} = 408.1 \pm 9.7$ Ω) or *f17* ($\Delta R_{ct} = 394.5 \pm 0.9$ Ω) sequences (Fig. 4B). However, single-base mismatch (*f17-1M*) and two-base mismatch (*yaiO-2M*) strand generated respectively only ~ 3% ($\Delta R_{ct} = 26.0 \pm 11.8$ Ω) and ~ 4% ($\Delta R_{ct} = 38.1 \pm 0.8$ Ω) hybridization efficiency, thus demonstrating very high differentiation between the fully matched and the single- and double-nucleotide polymorphism. Moreover, mixture of target DNA and 1-mismached or 2-mismached sequences provided similar responses, i.e., ~ 51% ($\Delta R_{ct} = 466.9 \pm 22.1$ Ω) for *yaiO/f17-1M* and ~ 40% ($\Delta R_{ct} = 358.3 \pm 5.5$ Ω) for *f17/yaiO-2M* mixtures, to those measured for target *yaiO* or *f17* alone, indicating the absence of interference by the mismatched DNA targets. Furthermore, a slight change in R_{ct} value was registered after incubation with either non-complementary sequence (~ 5%; $\Delta R_{ct} = 43.3 \pm 0.6$ Ω) or mixture of *yaiO-2M/f17-1M* DNA (~ 9%; $\Delta R_{ct} = 86.3 \pm 1.9$ Ω), which can be attributed to lower hybridization efficiency. Thereby, the proposed impedimetric DNA dual biosensor provided high selectivity for the simultaneous determination of *yaiO* and *f17* sequences.

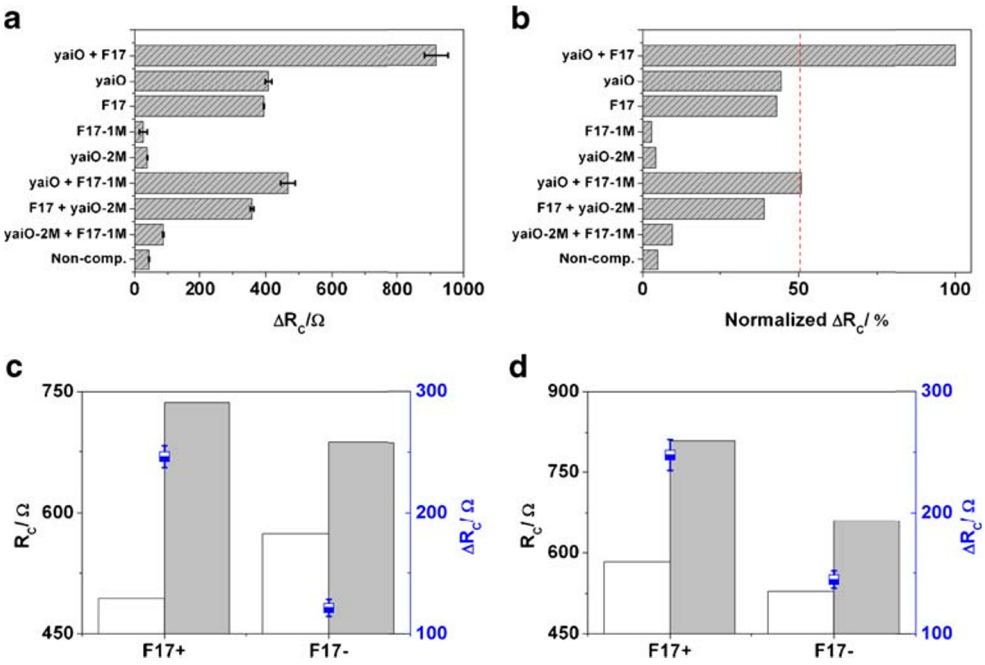

Fig. 4 Value of ΔR_{ct} (**A**) and normalized ΔR_{ct} (**b**) after hybridization with 100 pM of *yaiO/f17*mixture, *yaiO*, *f17*, *f17-1M*, *yaiO-2M*, *yaiO/f17-1M* mixture, *f17/yaiO-2M* mixture, *yaiO-2M/f17-1M* mixture, and non-complementary DNA targets; error bars, SD, $n = 3$. The R_{ct} value was measured before (white bars) and after (gray bars) hybridization with *f17*-positive and *f17*-negative samples from the whole (**c**) and digested (**d**) bacterial *E. coli* strains. Error bars, SD, $n = 3$

Detection of bacterial *E. coli* DNA

To assess the usefulness of the proposed procedure, the bioelectrode was used to detect *yaiO* and *f17* genes in extracted genomic DNA from *E. coli* strains isolated from diarrheic and healthy camel calves in Tunisia. PCR was used to identify *f17*-positive and *f17*-negative samples in order to provide a reliable validation for our approach. As displayed in Fig. 4C, a marked increase in charge transfer resistance value was registered after incubation with genomic *E. coli* strains indicating their complete hybridization (second and fourth columns). Moreover, ΔR_{ct} increased by a factor of almost 2 from 245.8 ± 8.9 Ω in the presence of *f17*-positive sample to 121.3 ± 7.3 Ω when compared to *f17*-negative sample, which indicated the successful detection of both *yaiO* and *f17* genes in the positive sample while only *yaiO* gene was determined in the negative sample. These results indicated that the developed procedure is in good agreement with the PCR assay.

To further increase the sensitivity, digestion with a restriction enzyme of *E. coli* genomic DNA was performed to get shorter DNA sequences. The same impedance behavior was recorded when the dual biosensor was incubated with *f17*-positive and *f17*-negative digested DNA samples (Fig. 4D). However, negligible changes in ΔR_{ct} values were recorded when compared to untreated whole DNA, revealing the sensitivity of the fabricated biosensor. These results strongly demonstrated that the developed biosensor is applicable for the simultaneous determination of *yaiO* and *f17* genes in genomic *E. coli* DNA without the need for enzymatic fragmentation, which allow cutting the cost of the procedure.

Conclusion

We designed a label-free DNA impedimetric dual biosensor using gold nanoparticle-modified SPCEs to simultaneously detect *E. coli*, i.e., *yaiO* gene, and its virulent *f17* fimbriae. Exploiting the electro-mechanical properties of the AuNPs, and potential-assisted immobilization strategy for the tethering of DNA dual-probe sequence, we achieved the detection in a very short time. The fabricated genosensor was able to detect both target DNA sequences in *E. coli* untreated and digested genomic DNA. Furthermore, the same amenable approach can be generalized to target other *E. coli* strains namely Shiga toxin-producing *E. coli* (i.e., O157, O145, or O104) or other bacteria of interests where the type of the bacterium and its strains is needed to be accurately identified.

Acknowledgments The Tunisian Ministry of Higher Education and Scientific Research (LR99ES15), the PRF program (NanofastResponse, grant ref.: PRF2017-D4P1 and SmartBioSens, grant ref.: PRFCOV19-D2P2 and COVID-PP grant ref.: PRFCOV19-D3P1), and the PHC Maghreb program (grant ref.: 39382 RE) are gratefully acknowledged.

Compliance with ethical standards All institutional and national guidelines for the care and use of laboratory and livestock animals were followed.

Conflict of interest The authors declare that they have no conflict of interest.

References

1. Knutton S, Lloyd DR, Candy D, Mcneish AS (1985) Adhesion of enterotoxigenic Escherichia coli to human small intestinal enterocytes. Infect Immun 48:824–831

2. Bertin Y, Martin C, Oswald E, Girardeau JP (1996) Rapid and specific detection of F17−related pilin and adhesin genes in diarrheic and septicemic Escherichia coli strains by multiplex PCR. J Clin Microbiol 34:2921–2928
3. Bessalah S, Fairbrother JM, Salhi I, Vanier G, Khorchani T, Seddik MM, Hammadi M (2016) Antimicrobial resistance and molecular characterization of virulence genes, phylogenetic groups of Escherichia coli isolated from diarrheic and healthy camel−calves in Tunisia. Comp Immunol Microbiol Infect Dis 49:1–7
4. Umpiérrez A, Acquistapace S, Fernández S, Oliver M, Acuña P, Reolón E, Zunino P (2016) Prevalence of Escherichia coli adhesion −related genes in neonatal calf diarrhea in Uruguay. J Infect Dev Ctries 10:472–477
5. Jamali H, Krylova K, Aïder M (2018) Identification and frequency of the associated genes with virulence and antibiotic resistance of Escherichia coli isolated from cow's milk presenting mastitis pathology. Anim Sci J89:1701–1706
6. Mainil JG, Gérardin J, Jacquemin E (2000) Identification of the F17 fimbrial subunit− and adhesin−encoding (f17A and f17G) gene variants in necrotoxigenic Escherichia coli from cattle, pigs and humans. Vet Microbiol 73:327–335
7. Bart S, Schwanitz A, Bauerfeind R (2011) Polymerase chain reaction−based method for the typing of F18 fimbriae and distribution of F18 fimbrial subtypes among porcine Shiga toxin−encoding Escherichia coli in Germany. J Vet Diagn Investig 23:454–464
8. Wang W, Zijlstra RT, Gänzle MG (2017) Identification and quantification of virulence factors of enterotoxigenic Escherichia coli by high −resolution melting curve quantitative PCR. BMC Microbiol 17:114
9. Bekal S, Brousseau R, Masson L, Prefontaine G, Fairbrother J, Harel J (2003) Rapid identification of Escherichia coli pathotypes by virulence gene detection with DNA microarrays. J Clin Microbiol 41:2113–2125
10. Jiang K, ZhuY LW, Feng Y, He L, Guan W, Hu W, Shi D (2012) Development of a loop−mediated isothermal amplification (LAMP) for the detection of F5 fimbriae gene in enterotoxigenic Escherichia coli (ETEC). Curr Microbiol 65:633–638
11. Torrente-Rodríguez RM, Campuzano S, Montiel VR-V, Gamella M, Pingarrón JM (2016) Electrochemical bioplatforms for the simultaneous determination of interleukin (IL)−8 mRNA and IL−8 protein oral cancer biomarkers in raw saliva. Biosens Bioelectron 77:543–548
12. Wan H, Sun Q, Li H, Sun F, Hu N, Wang P (2015) Screen−printed gold electrode with gold nanoparticles modification for simultaneous electrochemical determination of lead and copper. Sensors Actuators B Chem 209:336–342
13. Wang J, Liu G, Merkoci A (2003) Electrochemical coding technology for simultaneous detection of multiple DNA targets. J Am Chem Soc 125:3214–3215
14. Liang RP, Tian XC, Qiu P, Qiu JD (2014) Multiplexed electrochemical detection of trypsin and chymotrypsin based on distinguishable signal nanoprobes. Anal Chem 86:9256–9263
15. Chang J, Wang X, Wang J, Li H, Li F (2019) Nucleic acid−functionalized metal−organic framework−based homogeneous electrochemical biosensor for simultaneous detection of multiple tumor biomarkers. Anal Chem 91:3604–3610
16. Chen J, Liu Z, Zheng Y, Lin Z, Sun Z, Liu A, Chen W, Lin XB (2017) Genotyping of hepatitis B virus based on dual−probe electrochemical biosensor. J Electroanal Chem 785:75–79
17. Xu S, Chang Y, Wu Z, Li Y, Yuan R, Chai Y (2020) One DNA circle capture probe with multiple target recognition domains for simultaneous electrochemical detection of miRNA−21 and miRNA −155. Biosens Bioelectron 149:111848
18. Fernandes AM, Zhang F, Sun X (2014) A multiplex nanoparticles −based DNA electrochemical biosensor for the simultaneous detection of Escherichia coli O157:H7 and Staphylococcus aureus. Int J Curr Microbiol App Sci 3(4):750–759
19. Li Y, Xiong Y, Fang L, Jiang L, Huang H, Deng J, Liang W, Zheng J (2017) An electrochemical strategy using multifunctional nanoconjugates for efficient simultaneous detection of Escherichia coli O157: H7 and Vibrio cholerae O1. Theranostics 7(4):935–944
20. Azzouzi S, Rotariu L, Benito AM, Maser WK, Ben Ali M, Bala C (2015) A novel amperometric biosensor based on gold nanoparticles anchored on reduced graphene oxide for sensitive detection of L−lactate tumor biomarker. Biosens Bioelectron 69:280–286
21. Alves RC, Pimentel FB, Nouws HPA, Marques RCB, González-García MB, MBPP O, Delerue-Matos C (2015) Detection of Arah1 (a major peanut allergen) in food using an electrochemical gold nanoparticle−coated screen−printed immunosensor. Biosens Bioelectron 64:19–24
22. Arduini F, Zanardi C, Cinti S, Terzi F, Moscone D, Palleschi G, Seeber R (2015) Effective electrochemical sensor based on screen −printed electrodes modified with a carbon black − Au nanoparticles composite. Sensors Actuators B Chem 212:536–543
23. Jambrec D, Gebala M, La Mantia F, Schuhmann W (2015) Potential−assisted DNA immobilization as a prerequisite for fast and controlled formation of DNA monolayers. Angew Chem Int Ed 54:15064–15068
24. Zouari M, Campuzano S, Pingarron JM, Raouafi N (2018) Ultrasensitive determination of microribonucleic acids in cancer cells with nanostructured-disposable electrodes using the viral protein p19 for recognition of ribonucleic acid/microribonucleic acid homoduplexes. Electrochim Acta 262:39–47
25. Jaroenram W, Cecere P, Pompa PP (2019) Xylenol orange−based loop−mediated DNA isothermal amplification for sensitive naked −eye detection of Escherichia coli. J Microbiol Methods 156:9–14
26. Molin F, López-Acedo E, Tabla R, Roa I, Gómez A, Rebollo JE (2015) Improved detection of *Escherichia coli* and coliform bacteria by multiplex PCR. BMC Biotechnol 15:48
27. Lenzini L, Di Patti F, Lepri S, Livi R, Luccioli S (2020) Thermodynamics of DNA denaturation in a model of bacterial intergenic sequences. Chaos Solitons Fractals 130:109446
28. Shetti NP, Nayak DS, Malode SJ, Kulkarni RM (2017) An electrochemical sensor for clozapine at ruthenium doped TiO_2 nanoparticles modified electrode. Sensors Actuators B Chem 247:858–867
29. Kayra YU, Cinar N, Jambrec D, Schuhmann W (2018) Monitoring potential−induced DNA dehybridization kinetics for SNP detection using in−situ surface enhanced Raman scattering. Chem Electro Chem 5(5):756–760
30. Jambrec D, Kayran YU, Schuhmann W (2019) Controlling DNA/surface interactions for potential pulse−assisted preparation of multi −probe DNA microarrays. Electroanalysis 31:1–10
31. Shamsipur M, Samandari L, Taherpour AA, Pashabadi A (2019) Sub −femtomolar detection of HIV−1 gene using DNA immobilized on composite platform reinforced by a conductive polymer sandwiched between two nanostructured layers: a solid signal−amplification strategy. Anal Chim Acta 1055:7–16
32. Kotsiri Z, Vantarakis A, Rizzotto F, Kavanaugh D, Ramarao N, Vidic J (2019) Sensitive detection of E. coli in artificial seawater by aptamer −coated magnetic beads and direct PCR. Appl Sci 9(24):5392
33. Paniel N, Baudart J (2013) Colorimetric and electrochemical genosensors for the detection of Escherichia coli DNA without amplification in seawater. Talanta 115:133–142
34. Jaiswal N, Pandey CM, Solanki S, Tiwari I, Malhotra BD (2020) An impedimetric biosensor based on electrophoretically assembled ZnO nanorods and carboxylated graphene nanoflakes on an indium tin oxide electrode for detection of the DNA of Escherichia coli O157:H7. Microchim Acta 187:1